Respiratory heterogeneity shapes biofilm formation and host colonization in uropathogenic *Escherichia coli*

Running title: Respiratory heterogeneity in uropathogenic *Escherichia coli*

Connor J. Beebout,[a] Allison R. Eberly,[a] Sabrina H. Werby,[b] Seth A. Reasoner,[a] John R. Brannon,[a] Shuvro De,[c] Madison J. Fitzgerald,[d] Marissa M. Huggins,[d] Douglass B. Clayton,[c] Lynette Cegelski,[b] and Maria Hadjifrangiskou[a,e]#

[a]Department of Pathology, Microbiology, and Immunology, Vanderbilt University Medical Center, Nashville, TN, USA

[b]Department of Chemistry, Stanford University, Stanford, CA, USA

[c]Division of Pediatric Urology, Vanderbilt University Medical Center, Nashville, TN, USA

[d]Vanderbilt University, Nashville, TN, USA

[e]Vanderbilt Institute for Infection, Immunology & Inflammation, Vanderbilt University Medical Center, Nashville, TN, USA

#Address correspondence to: maria.hadjifrangiskou@vumc.org, @BacterialTalk

Abstract

Biofilms are multicellular bacterial communities encased in a self-secreted extracellular matrix comprised of polysaccharides, proteinaceous fibers, and DNA. Organization of these components lends spatial organization to the biofilm community such that biofilm residents can benefit from the production of common goods, while being protected from exogenous insults. Spatial organization is driven by the presence of chemical gradients, such as oxygen. Here we quantified and localized the expression of two *Escherichia coli* cytochrome oxidases in cells found in the biofilm state and defined their contribution to biofilm architecture. These studies elucidated a role for the high-affinity quinol oxidase cytochrome *bd* in matrix production and biofilm resident protection. Cytochrome *bd* was the most abundantly expressed respiratory complex in the biofilm community and was localized in the biofilm interior. Depletion of the cytochrome *bd*-expressing subpopulation led to decreased extracellular matrix and increased sensitivity of the community to exogenous stresses. Interrogation of the distribution of cytochrome oxidases in the planktonic state revealed that ~15% of the population expresses cytochrome *bd* at atmospheric oxygen concentration, and this population dominates during acute urinary tract infection. These data point towards a bet-hedging mechanism in which heterogeneous expression of respiratory complexes ensures respiratory plasticity of *E. coli* across diverse host niches.

Keywords

biofilms, heterogeneity, oxygen gradients, respiration, urinary tract infection

Importance

Biofilms are multicellular bacterial communities encased in a self-secreted extracellular matrix comprised of polysaccharides, proteinaceous fibers, and DNA. Organization of these components lends spatial organization in the biofilm community. Here we demonstrate that oxygen gradients in uropathogenic *Escherichia coli* (UPEC) biofilms lead to spatially distinct expression programs for cytochrome oxidases – components of the terminal electron transport chain. Our studies reveal that the cytochrome *bd*-expressing subpopulation is critical for biofilm development and matrix production. In addition, we show that cytochrome oxidases are also heterogeneously expressed in planktonic populations, and that this respiratory heterogeneity provides a fitness advantage during infection. These studies define the contributions of cytochrome oxidases to biofilm physiology and suggest the presence of respiratory bet-hedging behavior in UPEC.

Introduction

Rather than existing as a phenotypically uniform population, bacterial communities are characterized by subpopulations that are oftentimes phenotypically distinct. This intra-strain heterogeneity can be transient, brought about by stochastic differences in the abundance and activity of regulators in each individual cell, or it can be irreversible, through the acquisition of mutations. Heterogeneity influences the fate of the particular strain by allowing for at least a portion of the population to thrive in different niches as a result of its specific expression program.

Biofilms are complex multicellular communities assembled in an organized fashion in three-dimensional space. One of the most critical features of biofilms is a self-secreted extracellular matrix (ECM) that comprises a variety of exopolysaccharides, proteinaceous fibers, and extracellular DNA (1). The ECM protects the biofilm residents from predation, desiccation, assault by antimicrobial agents, and, when biofilms form in the host, the immune system. In addition to providing a physical barrier against external threats, the ECM also serves as a barrier to diffusion. Restricted diffusion, in conjunction with the metabolic activity of resident bacteria, leads to the establishment of various chemical gradients throughout the biofilm community (2, 3). Bacteria at different locales along the gradient respond to the microenvironment differently, and as a result differentiate into distinct and often metabolically cooperative subpopulations (3-7). Previous studies in *Pseudomonas aeruginosa* and *Escherichia coli* indicated that oxygen gradients play a key role in regulating the differential expression of genes involved in biofilm formation and metabolic specialization (8-11). The presence of an oxygen gradient suggests the emergence of subpopulations that utilize different respiratory components as a function of the oxygen abundance to which they are exposed. This leads to the hypothesis that the metabolic program of differentially respiring subpopulations is distinct from one another and contributes to differential production of biofilm goods that in turn enhance biofilm resilience.

Escherichia coli is a facultative anaerobe capable of utilizing multiple metabolic pathways to fulfill its energy requirements. In aerobically respiring *E. coli*, cytochrome oxidases comprise essential components of the terminal electron transport chain that couple the flow of electrons to the reduction of molecular oxygen into water (12, 13). *E.*

87 *coli* encodes two classes of cytochrome oxidases with differing oxygen affinities: one
88 heme copper oxidase, cytochrome *bo* (encoded by the *cyoABCD* gene cluster), and two
89 *bd*-type oxidases, cytochromes *bd* (*cydABX*) and bd_2 (*appBC*) (13, 14). Cytochrome *bo*
90 is induced at high (atmospheric, 21%) oxygen tensions, whereas the *bd*-type oxidases
91 are induced at low (hypoxic, 2-15%) oxygen tensions (13, 15). Based on these *in vitro*
92 expression patterns, we hypothesized that cytochrome *bo* would be enriched on the air-
93 exposed biofilm surface, whereas cytochromes *bd* and bd_2 would be enriched in the
94 hypoxic interior.

95 Here we report that the spatial distribution of cytochrome oxidases in biofilms
96 formed by uropathogenic *Escherichia coli* (UPEC) is a fundamental driver of biofilm
97 architecture. Peptide nucleic acid fluorescence *in situ* hybridization (PNA-FISH)
98 analyses assigned locations to each cytochrome-producing subpopulation, elucidating
99 for the first time spatially distinct expression programs for respiratory oxidases in *E. coli*.
100 Depletion of the cytochrome *bd*-expressing subpopulation from the biofilm significantly
101 impaired diffusion resistance by altering the abundance and organization of the ECM.
102 Assessment of deletion mutants in a well-established urinary tract infection murine
103 model revealed that only the cytochrome *bd* mutant was significantly attenuated for
104 virulence, although the infecting pool of bacteria in the parent strain exhibited
105 heterogeneous expression of all three respiratory oxidases. *In situ* analysis of urine-
106 associated bacteria demonstrated a shift of the population to cytochrome *bd* expression,
107 suggesting that the bladder favors cytochrome *bd*-expressing bacteria and that
108 heterogeneity in the input pool provides a fitness advantage to uropathogenic strains.
109 Our studies, performed on one of the most commonly acquired human pathogens and a

prolific biofilm producer *in vivo*, unveil a potential avenue for targeting heterogeneity and homogenizing bacterial programming as a therapeutic approach.

Results

Cytochrome bd is the most abundant respiratory transcript in mature UPEC biofilms

To test the hypothesis that multiple differentially respiring subpopulations exist in *E. coli* biofilms, we measured the relative expression of components of the aerobic (*cyoABCD*, *appBC*, and *cydABX*) and anaerobic (*napABC* and *narGHI*) respiratory chains in mature colony biofilms. Previous studies demonstrated that the central and peripheral regions of biofilms are metabolically distinct, yet co-dependent (16). The central region is shielded from environmental stressors and is therefore critical for survival of the population. The peripheral region contains a rapidly expanding population that contributes most to biofilm growth at the expense of being highly susceptible to exogenous threats. We first analyzed transcript levels in the center and periphery of colony biofilms grown on Yeast Extract/Casamino Acids (YESCA) agar (Fig. 1a), a medium which induces expression of key matrix components (curli amyloid fibers, type 1 pili, secreted proteins Hu-α/β, cellulose) that are also critical for fitness in the urinary tract (10, 17-19). At both regions, of the five respiratory operons analyzed, over 90 percent of transcripts corresponded to aerobic respiratory components (Fig. 1b-c). The most abundant transcript was that of *cydA* (Fig. 1b-d), corresponding to cytochrome *bd* complex (*cydABX*) expression. The *cydA* transcript levels were approximately 2-fold higher than those corresponding to *cyoABCD* (Fig. 1b-d), which was the second most highly abundant oxidase under the conditions tested. Cytochrome bd_2 was the third

133 most-highly expressed, while the anaerobic *narG* and *napA* genes exhibited baseline
134 expression levels (Fig. 1b-d). These results validated that most of the biofilm is hypoxic,
135 consistent with previous work in *P. aeruginosa* and *E. coli* (8, 9).
136
137 *Spatial organization of cytochrome expression along the oxygen gradient*

138 Previous studies elucidated the presence of steep biofilm oxygen gradients as a
139 function of biofilm depth (Fig. 2a) (8, 9). To define the spatial distribution of cytochrome-
140 expressing subpopulations, we performed PNA-FISH on cryosections of mature colony
141 biofilms using probes targeting each cytochrome oxidase operon (*cyoA*, *appC*, and
142 *cydA*) as well as *rrsH* as an endogenous control. Each PNA-FISH probe was designed
143 using the validated probe sequences used for qPCR (Fig. 1 and Table S1) to ensure
144 comparable hybridization efficiencies for each probe. SYTO 9 staining of sections was
145 used as an additional control to localize the entire biofilm community and account for
146 possible hybridization inconsistencies with the *rrsH* control probe (Figs. 2d, j and S1).
147 Consistent with previous observations demonstrating that the highest oxygen
148 abundance is at the air-exposed surface of the biomass (8, 9), we observed that
149 *cyoABCD* transcript was most abundant in bacteria lining the air-exposed surface of the
150 biofilm (Fig. 2b-c, f, h-i, l, n). In contrast, the highest abundance of *cydABX* transcript
151 was found in densely packed clusters of bacteria in the interior of the biofilm (Fig. 2b-c,
152 e, g, i, k, m). Interestingly, while in K12 *E. coli* the function of cytochrome *bd* and bd_2 are
153 thought to be redundant, the expression distribution of the two gene clusters was
154 different, with *appBC* observed to be evenly distributed throughout the community (Fig.
155 S1).

156

157 *Loss of cytochrome bd alters biofilm architecture, development, and matrix abundance*

158 The highly regulated spatial expression of cytochrome *bo* and cytochrome *bd*
159 oxidases in the biofilm raised the hypothesis that each of these cytochrome-expressing
160 subpopulations uniquely contributes to overall biofilm architecture. To test this
161 hypothesis, we created isogenic deletion mutants lacking the *cyoAB*, *appBC*, or *cydAB*
162 genes and compared the biofilms formed by the resulting strains (Fig. 3a). Colony
163 biofilms formed by the parental strain expand to an average diameter of 16.8 mm over
164 an 11-day incubation period and exhibit elaborate rugose architecture with distinct
165 central and peripheral regions (Figs. 3a and S2). Strains deleted for *cyoAB* and *appBC*
166 exhibited inverse phenotypes to each other, with the Δ*cyoAB* colony biofilms expanding
167 more than the parental strain (average diameter: 19.9 mm) and the Δ*appBC* colony
168 biofilms appearing more compact and with apparently higher rugosity (Figs. 3a and S2).
169 Strikingly, while Δ*cyoAB* and Δ*appBC* only displayed minor architectural changes,
170 Δ*cydAB* colony biofilms exhibited pronounced defects both in development and
171 architecture (Fig. 3a and S2). Colonies deleted for *cydAB* grew at a similar rate as the
172 parent, Δ*cyoAB*, and Δ*appBC* for the first 72 hours (Fig. S2). However, colony growth
173 was significantly stunted between days 3 and 11, with radial expansion remaining at an
174 average diameter of 10.3 mm and colonies exhibiting a wet mass of 48.11 mg (70% of
175 the parent strain) at the end of the experiment, even though the CFU produced by the
176 two strains were comparable across the 11-day incubation period (Figs. 3b-c and S2).
177 Complementation of Δ*cydAB* with an extra-chromosomal construct expressing *cydABX*
178 under its native promoter rescued the deletion phenotype, indicating that the defects

observed in the Δ*cydAB* mutant stem solely from the removal of the *cydABX* cluster (Fig. S3). Together, these observations demonstrate that cytochrome *bd* is a key contributor to biofilm development and suggest that loss of *cydAB* alters the synthesis and organization of the ECM.

Under the conditions used, the ECM of *E. coli* comprises primarily of cellulose and curli amyloid fibers (20). Previous solid-state nuclear magnetic resonance (NMR) spectroscopy analyses on intact ECM material defined the contributions of cellulose and curli to the *E. coli* biofilm ECM, and determined that curli and cellulose are present in a 6 to 1 ratio (20). More recently, the ECM cellulose was determined to be a chemically modified form of cellulose, specifically phosphoethanolamine (pEtN) cellulose (21). To interrogate the effects of *cydAB* deletion on curli and exopolysaccharide production, we extracted ECM and performed solid-state NMR analysis to evaluate the abundance of curli and cellulose components (Fig. 3d-e). The NMR spectra obtained for the parent and Δ*cydAB* ECM are very similar overall, indicating a comparable protein to polysaccharide ratio between the samples (Fig. 3d). Consistent with this analysis, we observe no change in protein composition between the parent and Δ*cydAB* ECM samples when analyzed on SDS-PAGE gels (Fig. 3e). We additionally do not observe any overt alterations to curli abundance or localization between UTI89 and Δ*cydAB* biofilm cryosections using immunofluorescence (Fig. 3f). Despite the similar composition, the total amount of ECM recovered was reduced in Δ*cydAB*, indicative of a decrease in ECM production. Because the protein to polysaccharide ratio and curli abundance are unchanged between the parent and Δ*cydAB*, these data are suggestive

of a change to the overall mixture of matrix components in Δ*cydAB*, with particular reductions in the abundance of non-curli and non-pEtN cellulose ECM components.

The ECM plays a central role in biofilm physiology by providing physical protection against exogenous insults, serving as a structural scaffold, and helping to establish chemical gradients which lead to metabolic differentiation and subpopulation formation (2, 3, 17, 22). As such, disruptions to the matrix can have catastrophic consequences for the biofilm community. We hypothesized that the altered matrix abundance and architecture in the Δ*cydAB* mutant would render the biofilm more susceptible to exogenous insults. To investigate this possibility, we probed the barrier function of the cytochrome oxidase mutant biofilms by applying a drop of colored water to the surface of mature colony biofilms (Fig. 3g and Movies S1-4) (23). While the parent strain, Δ*cyoAB*, and Δ*appBC* biofilms repelled the drop, the solution readily penetrated Δ*cydAB* biofilms, demonstrating that the alterations to Δ*cydAB* biofilm architecture and matrix abundance increases penetrance of aqueous solutions.

Loss of cytochrome bd increases population sensitivity to nitrosative stress under ambient oxygen concentrations

Together, our studies indicate that cytochrome *bd* is highly expressed in biofilms, and that loss of the cytochrome *bd*-expressing subpopulation impairs barrier function and reduces the abundance of extracellular matrix. These data suggest that the cytochrome *bd*-expressing subpopulation plays a critical role in promoting ECM synthesis and providing structural integrity to the community. However, it is also

possible that cytochrome *bd* is preferentially expressed in the biofilm because cytochrome *bd* provides protection against oxidative and nitrosative stress – byproducts of biofilm metabolism (24, 25) and, in the case of infection, components of the innate immune response (26-28). Previous studies demonstrated that cytochrome *bd* has catalase activity, is capable of oxidizing the respiratory inhibitor nitric oxide, and is insensitive to nitrosative stress due to its unusually fast nitric oxide dissociation rate (26). These biochemical activities are thought to occur at unique locations on the protein; quinol oxidation occurs at the periplasmic Q loop, oxygen reduction and nitric oxide binding occurs at heme *d*, and catalase activity is thought to occur through heme b_{595} (14, 29, 30). By contrast, cytochrome *bo* affords no protection against oxidative or nitrosative stress and is irreversibly inhibited by nitric oxide (26). Given these additional functions of cytochrome *bd*, we performed growth curves at ambient oxygen concentration and evaluated the effects of nitrosative and oxidative stress on the fitness of cells lacking *cydAB* or *cyoAB* as compared to the parent strain. Without the addition of stress, both mutants exhibited a lag in growth (Fig. 4a), but each reached a maximal CFU/mL similar to the parental strain by the end of the growth experiment (Fig. 4a). ATP measurements of the corresponding cultures revealed no significant overall differences in ATP concentrations between the strains during logarithmic growth (Fig. 4b). Next, to determine whether loss of cytochrome *bd* impairs resistance to oxidative and nitrosative stress, we measured growth with and without these stressors. Whereas treatment with H_2O_2 had no significant effects on the growth of the two mutants (Fig. 4c), addition of the nitric oxide donor NOC-12 to planktonic cultures most significantly impacted growth of Δ*cydAB* (Fig. 4d), consistent with previous studies on K12 *E. coli*

and the multi-drug resistant strain ST131 (27, 28). Together, these data demonstrate that while cytochrome *bd* is dispensable for energy generation during planktonic growth, loss of cytochrome *bd* sensitizes bacteria to nitrosative stress. In conjunction with the disrupted biofilm architecture and altered matrix abundance in Δ*cydAB* biofilms, these data suggest that cytochrome *bd*-expressing subpopulations are critical, not only for directing matrix biosynthesis, but also for withstanding harmful metabolic byproducts while in the biofilm state.

Heterogeneous expression of cytochrome oxidases at the population level

Our data thus far indicate that in addition to heterogeneity in cytochrome oxidase expression in the biofilm state, heterogeneous expression of cytochrome oxidases must also be occurring in the planktonic population. Our planktonic studies revealed a lag in growth of the Δ*cyoAB* and the Δ*cydAB* mutants when these strains were grown under ambient oxygen concentrations, suggesting that in a given culture there are subpopulations – like in the biofilm – that stochastically or deterministically express different respiratory components. Such a bet-hedging approach could provide UPEC with the flexibility to quickly adapt to a given niche, be it different locales in the genitourinary tract or in the gastrointestinal tract during host colonization. In the context of urinary tract infection, *E. coli* traverse from the nearly anoxic gut to the perineum, where it encounters atmospheric oxygen concentrations, prior to ascending the urethra to enter the hypoxic bladder, where the dissolved urinary oxygen concentration is 4 – 6% (31). This microbial journey is performed by planktonic cells, which can then expand

268 into multicellular communities on and within bladder epithelial cells, as well as on
269 urinary catheters (1, 32). In previous studies, we and others demonstrated that UPEC
270 respire aerobically during infection (33-35) and that biofilm formation is favored in
271 conditions that mimic oxygen levels in the bladder (36).

272 The high abundance of *cydABX* transcript in the hypoxic areas of the biofilm, in
273 conjunction with the defects observed in aerobically grown Δ*cydAB* planktonic cultures,
274 raised the hypothesis that a cytochrome *bd*-expressing subpopulation exists in the
275 planktonic state under ambient oxygen conditions and that this cytochrome *bd*-
276 expressing subpopulation exhibits the greatest fitness advantage during infection. To
277 test this hypothesis, we first analyzed transcript abundance in cultures used for
278 inoculation during murine infections with qPCR and PNA-FISH (Fig. 5). Under these
279 conditions, qPCR analysis indicated that the majority of transcript corresponds to
280 *cyoABCD* (69.7%), with *cydABX* and *appBC* transcripts each comprising approximately
281 15% of detected transcripts (Fig. 5a). Transcript abundance was altered by decreasing
282 ambient oxygen concentrations, with the most abundant transcript corresponding to
283 *cydABX* in 12%, 8% and 4% oxygen, the latter being the concentration of dissolved
284 oxygen concentration in the urine (Figs. 5a-b and S4) (31). PNA-FISH analysis revealed
285 the presence of bacteria which uniquely express cytochrome *bo* (Fig. 5f), *bd* (Fig. 5e),
286 or bd_2 (Fig. 5g), as well as some cells that have transcript of all three operons (Fig. 5c,
287 e-g). Intriguingly, we observed dividing cells in which each daughter had distinct
288 cytochrome oxidase transcript abundance (Fig. 5c, inset), suggesting that asymmetric
289 distribution of respiratory transcripts during division may be a mechanism by which
290 these subpopulations are generated.

Expression of cytochrome bd is dominant during acute urinary tract infection

Previous studies reported that deletion of cytochrome *bd* impairs UPEC virulence in a UTI model (28). To gauge the contribution of each cytochrome oxidase during infection, we evaluated the fitness of Δ*cyoAB,* Δ*appBC*, and Δ*cydAB* mutants compared to the parent strain in a murine model of acute urinary tract infection. Consistent with the previous report (28), Δ*cydAB* exhibited a ~2 log decrease in bladder colonization by 24 hours relative to the parent strain, while the mutants deleted for *cyoAB* and *appBC* colonize mice at the same level as the parent strain (Fig. 5m). Subsequent PNA-FISH on pooled urine obtained from mice infected with the parent strain revealed a marked enrichment in cytochrome *bd*-expressing cells and a corresponding reduction in the number of cells expressing cytochrome *bo* (Fig. 5h-l). This suggests that the bladder environment either induces transcription of *cydABX* or that only subpopulations of bacteria expressing *cydABX* are capable of efficiently colonizing the bladder. Together these data reveal the presence of subpopulations of bacteria that differentially express cytochrome oxidases as a potential bet-hedging mechanism to promote bladder colonization.

Discussion

Cytochrome *bd* is a multifunctional protein that is central to respiration and can maintain activity in the face of nitrosative stress (26). As such, bacteria expressing cytochrome *bd* presumably exhibit a fitness advantage during growth conditions that are

low in oxygen or high in metabolic byproducts that increase nitric oxide concentration. The biofilm state, while protecting the bacterial residents from predation and desiccation, constitutes a high-density environment with several chemical gradients that result from the consumption and production of metabolites. Accordingly, expressing an enzyme that can facilitate tolerance to metabolic byproducts, such as nitric oxide, would ensure that biofilm residents do not perish as a consequence of their own metabolic excretions. Our study elucidates the distribution of cytochrome oxidase expression in the biofilm state and indicates that the bulk of biofilm residents express cytochrome *bd*, particularly in the densely populated interior. The cytochrome *bd*-expressing bacteria are not necessarily using cytochrome *bd* for respiration, as many of them also have low levels of cytochrome *bo* and bd_2 transcripts (Fig. 2 and S1). Rather, the production of cytochrome *bd* may be leveraged towards providing tolerance to nitrosative stress, which irreversibly inhibits cytochrome *bo*. Indeed, in Δ*cydAB* biofilms we observe a marked increase in cytochrome *bo* expression (Fig. S5), suggesting that loss of cytochrome *bd* impairs nitric oxide tolerance and that increased production of cytochrome *bo* may be a compensatory mechanism that allows biofilm bacteria to respire in the presence of high levels of nitric oxide.

In addition to acting as a respiratory inhibitor, nitric oxide regulates cyclic di-GMP abundance and thereby governs the switch from motility to aggregation and biofilm expansion (37, 38). Consequently, if cytochrome *bd* decreases nitric oxide availability, it would indirectly influence ECM production. Consistent with this hypothesis, loss of the cytochrome *bd*-expressing subpopulation reduces the total abundance of matrix components and leads to gross alterations of biofilm architecture (Fig. 3). It is thus

336 possible that the cytochrome *bd*-expressing subpopulation is critical for promoting the
337 biosynthesis of the ECM by influencing the nitric oxide – cyclic di-GMP signaling axis.
338 We are currently investigating this possibility.

339 Most importantly, this work revealed the presence of planktonic subpopulations
340 that express distinct cytochrome oxidases during growth. In conjunction with the
341 observation that only cytochrome *bd* expression is critical for fitness during infection,
342 this finding suggests that basal expression of cytochrome *bd* under aerobic conditions
343 serves as a bet-hedging mechanism that promotes the expansion of bacteria during the
344 transition from the aerobic perineum to the hypoxic bladder. In addition to allowing for
345 efficient respiration in the hypoxic bladder, expression of cytochrome *bd* provides
346 resistance against nitrosative stress – a metabolic byproduct and component of the
347 innate immune response – and promotes the formation of resilient biofilm communities.
348 These observations suggest the presence of respiratory bet-hedging behavior in UPEC,
349 and additionally suggest the possibility of targeting heterogeneity as a method for
350 homogenizing bacterial populations and impeding their ability to colonize the urinary
351 tract.

352

353 **Materials and Methods**

354 Bacterial Strains

355 All studies were performed in *Escherichia coli* cystitis isolate UTI89 (39). All gene
356 deletions (Δ*cyoAB*, Δ*appBC*, and Δ*cydAB*) were performed using the λ-red
357 recombinase system (40). Complementation constructs were created in plasmid

358 pTRC99a with *cydABX* under the control of its native promoter as previously described
359 (41). Primers used for gene deletions and complementation plasmid construction are
360 listed in Table S1.
361
362 Growth conditions
363 For all analyses, strains were propagated overnight at 37°C with shaking in Lysogeny
364 broth (LB) (Fisher) at pH 7.4. To form colony biofilms, 10 µL of overnight culture was
365 spotted onto 1.2x Yeast Extract/Casamino Acids (YESCA) agar (9) and allowed to grow
366 at room temperature. Growth curves to assess tolerance to nitrosative or oxidative
367 stress were performed in LB broth at 37˚C with shaking, starting from an overnight
368 culture normalized to optical density at 600 nm (OD_{600}) = 0.05. At 2 hours post-
369 inoculation, cultures were split into equal volumes and treated with 0.5 mM NOC-12, 1
370 mM H_2O_2, or left unperturbed. OD_{600} and CFU per mL measurements were taken every
371 hour for 8 hours.
372
373 RT-qPCR
374 RNA was extracted from day 11 colony biofilms or planktonic cultures using the RNeasy
375 kit (Qiagen). RNA was DNase treated using Turbo DNase I (Invitrogen), and reverse
376 transcribed using SuperScript III Reverse Transcriptase (Invitrogen). cDNA was
377 amplified in an Applied Biosystems StepOne Plus Real-Time PCR machine using
378 TaqMan MGB chemistry with the primers and probes listed in Table S1. All reactions
379 were performed in triplicate with four different cDNA concentrations (100, 50, 25, or 12.5
380 ng per reaction). Relative fold difference in transcript abundance was determined using

the $\Delta\Delta C_T$ method (42) with target transcripts normalized to *gyrB* abundance from a total of 3 – 4 biological replicates.

Peptide nucleic acid fluorescence *in situ* hybridization (PNA-FISH)

Day 11 biofilms were flash frozen in Tissue-Tek O.C.T. compound (Electron Microscopy Sciences) and cryosectioned as described previously (5). The PNA-FISH hybridization protocol was adapted from Almeida *et al* (43). Biofilm cryosections were fixed in 4% paraformaldehyde (PFA) for 30 minutes at room temperature, then dehydrated for 10 minutes in 50% ethanol. After dehydration, 100 µL of hybridization solution (see below for details) was applied to the slides. All hybridizations were performed at 60˚C for 30 minutes. Next, slides were submerged in pre-warmed wash solution for 30 minutes, mounted using ProLong Diamond (ThermoFisher), and imaged using a Zeiss 710 confocal laser scanning microscope (CLSM). For planktonic cells, 1 mL of culture was sedimented, fixed in 4% PFA, resuspended in 50% ethanol, incubated at -20˚C for 30 minutes, and resuspended in 100 µL hybridization solution. After hybridization, cells were pelleted, resuspended in 500 µL pre-warmed wash solution, and incubated at 60˚C for 30 minutes. Finally, cells were pelleted and resuspended in 100 µL sterile water before being applied to microscope slides for imaging. Wash solution contained 5 mM Tris-HCl pH 7.4, 15 mM NaCl, and 1% Triton X-100. Hybridization solution contained 10% w/v dextran sulfate, 30% formamide, 50 mM Tris-HCl pH 7.4, 10 mM NaCl, 5 mM EDTA, 0.1% Triton X-100, and 200 nM of each PNA-FISH probe. Probe sequences were based on the probes used for qPCR (efficiency of hybridization: *rrsH*:

403 81; *cydA*: 107; *cyoA*: 115; *appC*: 73) and were synthesized by PNA Bio (Newbury Park,
404 CA).
405
406 ATP measurements
407 ATP was quantified from mid-log (4 hours after subculture) planktonic cultures using
408 Cell-Glo Titer kit (Promega). Cultures were normalized to OD_{600} = 0.5, pelleted, and
409 resuspended in PBS. 50 µL of bacterial suspension was mixed with an equal volume of
410 Cell-Glo Titer reagent and incubated shaking at room temperature for 15 minutes. After
411 incubation, luminescence was measured on a SpectraMax i3 plate reader (Molecular
412 Devices). Luminescence was converted to concentration of ATP using a standard curve
413 on the same plate.
414
415 Extracellular matrix extraction
416 Extracellular matrix was extracted using established methods (20). Briefly, biofilms were
417 grown on YESCA agar containing 25 µg/mL Congo Red. After 60 hours, biofilms were
418 homogenized in cold 10 mM Tris-HCl pH 7.4 using an Omni Tissue Homogenizer
419 (motor speed 9) five times for one minute per cycle. Next, the homogenate was
420 centrifuged three times for 10 minutes at 5,000*g* to remove cells. The supernatant was
421 spiked with NaCl (final concentration 170mM) and centrifuged for one hour at 13,000*g*
422 to pellet the matrix. The ECM pellet was washed in 10 mM Tris-HCl pH 7.4 with 4%
423 SDS and incubated at room temperature rocking overnight. Next, the suspended ECM
424 was centrifuged at 13,000*g* for one hour, resuspended in cold 10 mM Tris-HCl pH 7.4,

and centrifuged at 30,000*g* for 20 minutes. Pelleted ECM was resuspended in MQ water and flash frozen.

Solid-state NMR Measurements

All NMR experiments were performed in an 89 mm bore 11.7T magnet using either an HCN Agilent probe with a DD2 console (Agilent Technologies) or a home-built four-frequency transmission line probe with a Varian console. Samples were spun at 7143 Hz in either 36 µL capacity 3.2 mm Zirconia rotors or thin-walled 5 mm outer diameter Zirconia rotors. The temperature was maintained at 5˚C with an FTS chiller (FTS Thermal Products, SP Scientific, Warminster, PA) supplying nitrogen at -10˚C. The field strength for ^{13}C cross polarization was 50 kHz with a 10% ^{1}H linear ramp centered at 57 kHz. The CPMAS recycle time was 2 s for all experiments. ^{1}H decoupling was performed with continuous wave decoupling. ^{13}C chemical shifts were referenced to tetramethylsilane as 0 ppm using a solid adamantine sample at 38.5 ppm. The 15.6 mg wild-type ^{13}C CPMAS spectrum was the result of 32,768 scans and the 8.3 mg mutant spectrum was the result of 100,000 scans. NMR spectra were processed with 80 Hz line broadening.

SDS-PAGE gels

A portion of the lyophilized ECM sample used for solid-state NMR analysis was resuspended in 98% formic acid and vacuum centrifuged. The samples were then reconstituted in SDS-PAGE sample buffer containing 8M urea and 50 mM DTT and further diluted to desired concentrations. All samples were centrifuged briefly at 10,000*g*

448 to remove any insoluble material and used for electrophoresis. The gels were stained
449 with instant blue and de-stained in water.
450
451 Immunofluorescence
452 Immunofluorescence targeting CsgA, the major curli subunit, was performed as
453 previously described (10). Biofilm cryosections were fixed in 4% PFA for 30 minutes at
454 room temperature and blocked overnight in 5% BSA at 4˚C. Sections were washed in
455 PBS, incubated with rabbit α-CsgA antibodies (GenScript) (1:1000) at room temperature
456 for 1 hour, washed in PBS, and incubated with AlexaFluor 647 goat α-rabbit IgG
457 (ThermoFisher) (1:1000) at room temperature for 1 hour. Slides were counterstained
458 with SYTO 9 and imaged using CLSM.
459
460 Murine infections
461 Murine infections were performed as described previously (44). In brief, UTI89 and each
462 mutant strain were inoculated individually into 5 mL LB medium and grown shaking at
463 37˚C for 4 hours. Next, this culture was diluted 1:1000 into 10 mL fresh media and
464 grown statically at 37˚C for 24 hours. After 24 hours, this culture was diluted 1:1000 into
465 10 mL fresh media and grown for another 24 hours at 37˚C statically. Next, 7 – 8 week
466 old C3H/HeN female mice were transurethrally inoculated with 50 µL PBS containing
467 10^7 CFU bacteria. Mice were sacrificed at 24 hours post infection after which bladders
468 were removed and homogenized for CFU enumeration. All animal studies were
469 approved by the Vanderbilt University Medical Center Institutional Animal Care and
470 Use Committee (IACUC) (protocol number M/12/191) and carried out in accordance

with all recommendations in the Guide for the Care and Use of Laboratory Animals of the National Institutes of Health and the IACUC.

Statistical analysis

All statistical analyses were performed in GraphPad Prism using the most appropriate test. Details of test used, error bars, and statistical significance cutoffs are presented in figure legends.

Acknowledgments

We thank Dr. Jonathan Schmitz, Dr. Gerald Van Horn, Dr. Mariana X. Byndloss, and members of the Hadjifrangiskou laboratory for critical evaluation of the manuscript and helpful discussions. This work was supported by the following NIH grants**:** R01 AI107052 (MH), DiaComp DK076169 (MH), T32 GM007347 (CJB), K08 DK106472 (DBC) and the Vanderbilt University Medical Center Pediatric Urology Research Fund. LC acknowledges support from the National Science Foundation CAREER Award 1453247. SHW is a recipient of a NSF Predoctoral Fellowship.

Author Contributions

CJB, ARE, and MH conceived the study, performed the experiments, analyzed the data, and composed the manuscript. SAR performed the nitrosative and oxidative stress assays. MJF and MMH constructed deletion mutants and complementation constructs under the supervision of CJB and ARE. JRB assisted with imaging data acquisition. SD and DBC performed the animal experiments along with CJB and ARE, assisted in data

494 analysis, and edited the manuscript. SHW and LC performed the extracellular matrix
495 component measurements and edited the manuscript.

496

497 **Declaration of Interests**

498 The authors declare no conflicts of interest at the time of submission of this manuscript.

499

500 **References**

501 1. Kostakioti M, Hadjifrangiskou M, Hultgren SJ. 2013. Bacterial biofilms:
502 development, dispersal, and therapeutic strategies in the dawn of the
503 postantibiotic era. Cold Spring Harb Perspect Med 3:a010306.
504 2. Stewart P, Franklin M. 2008. Physiological heterogeneity in biofilms, Nature
505 Reviews Microbiology.
506 3. Nadell CD, Drescher K, Foster KR. 2016. Spatial structure, cooperation and
507 competition in biofilms. Nat Rev Microbiol 14:589-600.
508 4. Stewart PS, Franklin MJ. 2008. Physiological heterogeneity in biofilms. Nat Rev
509 Microbiol 6:199-210.
510 5. Vlamakis H, Aguilar C, Losick R, Kolter R. 2008. Control of cell fate by the
511 formation of an architecturally complex bacterial community. Genes Dev 22:945-
512 53.
513 6. van Gestel J, Vlamakis H, Kolter R. 2015. Division of Labor in Biofilms: the
514 Ecology of Cell Differentiation. Microbiol Spectr 3:MB-0002-2014.

7. Dragoš A, Kiesewalter H, Martin M, Hsu CY, Hartmann R, Wechsler T, Eriksen C, Brix S, Drescher K, Stanley-Wall N, Kümmerli R, Kovács Á. 2018. Division of Labor during Biofilm Matrix Production. Curr Biol 28:1903-1913.e5.

8. Dietrich LE, Okegbe C, Price-Whelan A, Sakhtah H, Hunter RC, Newman DK. 2013. Bacterial community morphogenesis is intimately linked to the intracellular redox state. J Bacteriol 195:1371-80.

9. DePas WH, Hufnagel DA, Lee JS, Blanco LP, Bernstein HC, Fisher ST, James GA, Stewart PS, Chapman MR. 2013. Iron induces bimodal population development by Escherichia coli. Proc Natl Acad Sci U S A 110:2629-34.

10. Floyd KA, Moore JL, Eberly AR, Good JA, Shaffer CL, Zaver H, Almqvist F, Skaar EP, Caprioli RM, Hadjifrangiskou M. 2015. Adhesive fiber stratification in uropathogenic Escherichia coli biofilms unveils oxygen-mediated control of type 1 pili. PLoS Pathog 11:e1004697.

11. Jo J, Cortez KL, Cornell WC, Price-Whelan A, Dietrich LE. 2017. An orphan *cbb*$_3$-type cytochrome oxidase subunit supports *Pseudomonas aeruginosa* biofilm growth and virulence. Elife 6.

12. Unden G, Bongaerts J. 1997. Alternative respiratory pathways of Escherichia coli: energetics and transcriptional regulation in response to electron acceptors. Biochim Biophys Acta 1320:217-34.

13. Borisov VB, Verkhovsky MI. 2015. Oxygen as Acceptor. EcoSal Plus 6.

14. Borisov VB, Gennis RB, Hemp J, Verkhovsky MI. 2011. The cytochrome bd respiratory oxygen reductases. Biochim Biophys Acta 1807:1398-413.

15. Morris RL, Schmidt TM. 2013. Shallow breathing: bacterial life at low O(2). Nat Rev Microbiol 11:205-12.

16. Liu J, Prindle A, Humphries J, Gabalda-Sagarra M, Asally M, Lee DY, Ly S, Garcia-Ojalvo J, Süel GM. 2015. Metabolic co-dependence gives rise to collective oscillations within biofilms. Nature 523:550-4.

17. Cegelski L, Pinkner JS, Hammer ND, Cusumano CK, Hung CS, Chorell E, Aberg V, Walker JN, Seed PC, Almqvist F, Chapman MR, Hultgren SJ. 2009. Small-molecule inhibitors target Escherichia coli amyloid biogenesis and biofilm formation. Nat Chem Biol 5:913-9.

18. Jurcisek JA, Brockman KL, Novotny LA, Goodman SD, Bakaletz LO. 2017. Nontypeable. Proc Natl Acad Sci U S A 114:E6632-E6641.

19. Rapsinski GJ, Wynosky-Dolfi MA, Oppong GO, Tursi SA, Wilson RP, Brodsky IE, Tükel Ç. 2015. Toll-like receptor 2 and NLRP3 cooperate to recognize a functional bacterial amyloid, curli. Infect Immun 83:693-701.

20. McCrate OA, Zhou X, Reichhardt C, Cegelski L. 2013. Sum of the parts: composition and architecture of the bacterial extracellular matrix. J Mol Biol 425:4286-94.

21. Thongsomboon W, Serra DO, Possling A, Hadjineophytou C, Hengge R, Cegelski L. 2018. Phosphoethanolamine cellulose: A naturally produced chemically modified cellulose. Science 359:334-338.

22. Hufnagel DA, Depas WH, Chapman MR. 2015. The Biology of the Escherichia coli Extracellular Matrix. Microbiol Spectr 3.

559 23. Hobley L, Ostrowski A, Rao FV, Bromley KM, Porter M, Prescott AR, MacPhee
560 CE, van Aalten DM, Stanley-Wall NR. 2013. BslA is a self-assembling bacterial
561 hydrophobin that coats the Bacillus subtilis biofilm. Proc Natl Acad Sci U S A
562 110:13600-5.
563 24. Asally M, Kittisopikul M, Rué P, Du Y, Hu Z, Çağatay T, Robinson AB, Lu H,
564 Garcia-Ojalvo J, Süel GM. 2012. Localized cell death focuses mechanical forces
565 during 3D patterning in a biofilm. Proc Natl Acad Sci U S A 109:18891-6.
566 25. Cutruzzolà F, Frankenberg-Dinkel N. 2016. Origin and Impact of Nitric Oxide in
567 Pseudomonas aeruginosa Biofilms. J Bacteriol 198:55-65.
568 26. Giuffrè A, Borisov VB, Arese M, Sarti P, Forte E. 2014. Cytochrome bd oxidase
569 and bacterial tolerance to oxidative and nitrosative stress. Biochim Biophys Acta
570 1837:1178-87.
571 27. Mason MG, Shepherd M, Nicholls P, Dobbin PS, Dodsworth KS, Poole RK,
572 Cooper CE. 2009. Cytochrome bd confers nitric oxide resistance to Escherichia
573 coli. Nat Chem Biol 5:94-6.
574 28. Shepherd M, Achard ME, Idris A, Totsika M, Phan MD, Peters KM, Sarkar S,
575 Ribeiro CA, Holyoake LV, Ladakis D, Ulett GC, Sweet MJ, Poole RK, McEwan
576 AG, Schembri MA. 2016. The cytochrome bd-I respiratory oxidase augments
577 survival of multidrug-resistant Escherichia coli during infection. Sci Rep 6:35285.
578 29. Borisov VB, Forte E, Davletshin A, Mastronicola D, Sarti P, Giuffrè A. 2013.
579 Cytochrome bd oxidase from Escherichia coli displays high catalase activity: an
580 additional defense against oxidative stress. FEBS Lett 587:2214-8.

581 30. Safarian S, Rajendran C, Müller H, Preu J, Langer JD, Ovchinnikov S, Hirose T,
582 Kusumoto T, Sakamoto J, Michel H. 2016. Structure of a bd oxidase indicates
583 similar mechanisms for membrane-integrated oxygen reductases. Science
584 352:583-6.
585 31. Wang ZJ, Joe BN, Coakley FV, Zaharchuk G, Busse R, Yeh BM. 2008. Urinary
586 oxygen tension measurement in humans using magnetic resonance imaging.
587 Acad Radiol 15:1467-73.
588 32. Flores-Mireles AL, Walker JN, Caparon M, Hultgren SJ. 2015. Urinary tract
589 infections: epidemiology, mechanisms of infection and treatment options. Nat
590 Rev Microbiol 13:269-84.
591 33. Hadjifrangiskou M, Kostakioti M, Chen SL, Henderson JP, Greene SE, Hultgren
592 SJ. 2011. A central metabolic circuit controlled by QseC in pathogenic
593 Escherichia coli. Mol Microbiol 80:1516-29.
594 34. Floyd KA, Mitchell CA, Eberly AR, Colling SJ, Zhang EW, DePas W, Chapman
595 MR, Conover M, Rogers BR, Hultgren SJ, Hadjifrangiskou M. 2016. The UbiI
596 (VisC) Aerobic Ubiquinone Synthase Is Required for Expression of Type 1 Pili,
597 Biofilm Formation, and Pathogenesis in Uropathogenic Escherichia coli. J
598 Bacteriol 198:2662-72.
599 35. Alteri CJ, Smith SN, Mobley HL. 2009. Fitness of Escherichia coli during urinary
600 tract infection requires gluconeogenesis and the TCA cycle. PLoS Pathog
601 5:e1000448.
602 36. Eberly AR, Floyd KA, Beebout CJ, Colling SJ, Fitzgerald MJ, Stratton CW,
603 Schmitz JE, Hadjifrangiskou M. 2017. Biofilm Formation by Uropathogenic

604 Escherichia coli Is Favored under Oxygen Conditions That Mimic the Bladder
605 Environment. Int J Mol Sci 18.
606 37. Barraud N, Schleheck D, Klebensberger J, Webb JS, Hassett DJ, Rice SA,
607 Kjelleberg S. 2009. Nitric oxide signaling in Pseudomonas aeruginosa biofilms
608 mediates phosphodiesterase activity, decreased cyclic di-GMP levels, and
609 enhanced dispersal. J Bacteriol 191:7333-42.
610 38. Hengge R. 2009. Principles of c-di-GMP signalling in bacteria. Nat Rev Microbiol
611 7:263-73.
612 39. Mulvey MA, Schilling JD, Hultgren SJ. 2001. Establishment of a persistent
613 Escherichia coli reservoir during the acute phase of a bladder infection. Infect
614 Immun 69:4572-9.
615 40. Murphy KC, Campellone KG. 2003. Lambda Red-mediated recombinogenic
616 engineering of enterohemorrhagic and enteropathogenic E. coli. BMC Mol Biol
617 4:11.
618 41. Shaffer CL, Zhang EW, Dudley AG, Dixon BR, Guckes KR, Breland EJ, Floyd
619 KA, Casella DP, Algood HM, Clayton DB, Hadjifrangiskou M. 2017. Purine
620 Biosynthesis Metabolically Constrains Intracellular Survival of Uropathogenic
621 Escherichia coli. Infect Immun 85.
622 42. Pfaffl MW. 2001. A new mathematical model for relative quantification in real-
623 time RT-PCR. Nucleic Acids Res 29:e45.
624 43. Almeida C, Azevedo NF, Santos S, Keevil CW, Vieira MJ. 2011. Discriminating
625 multi-species populations in biofilms with peptide nucleic acid fluorescence in situ
626 hybridization (PNA FISH). PLoS One 6:e14786.

627 44. Hung CS, Dodson KW, Hultgren SJ. 2009. A murine model of urinary tract
628 infection. Nat Protoc 4:1230-43.

629

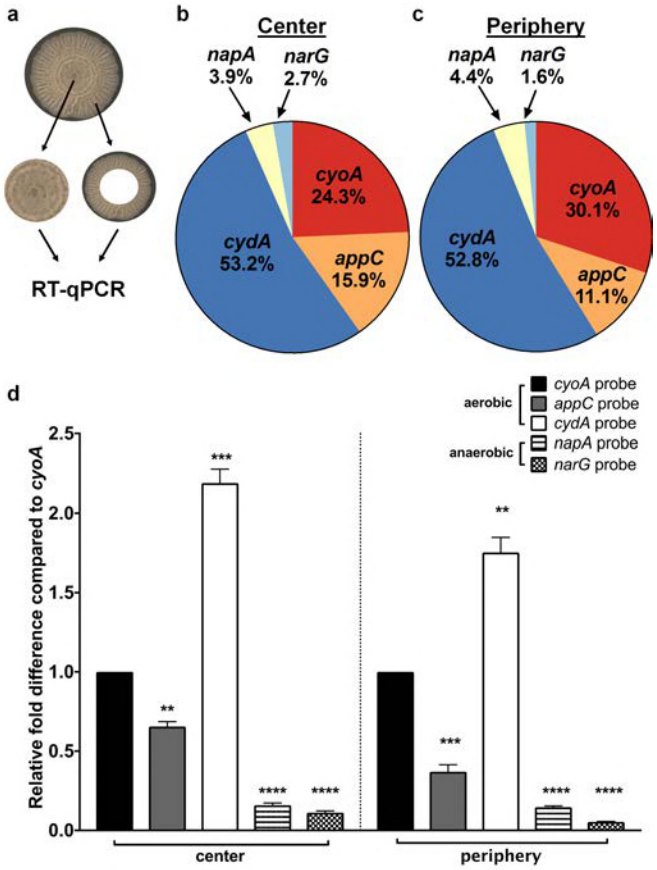

Figure 1: Lateral expression of respiratory complexes in *Escherichia coli* biofilms: a, Image of a mature colony biofilm formed by UPEC strain UTI89 on YESCA agar. The center and periphery of colony biofilms were harvested and subjected to RNA extraction and RT-qPCR using the following probes: *cydA, cyoA, appC, napA,* and *narG* with *gyrB* as a normalizer. **b – c,** Pie charts indicating the relative abundance of detected respiratory transcripts in the biofilm center (**b**) and periphery (**c**)**. d,** Graphs depicting relative fold differences in transcript abundance in the biofilm center and periphery. The graph and pie chart depict the average of 4 biological replicates. Statistical analysis was performed in GraphPad Prism using a two-tailed paired t test. Data are presented as mean ± SEM. * = $p < 0.05$, ** = $p < 0.01$, *** = $p < 0.001$, **** = $p < 0.0001$.

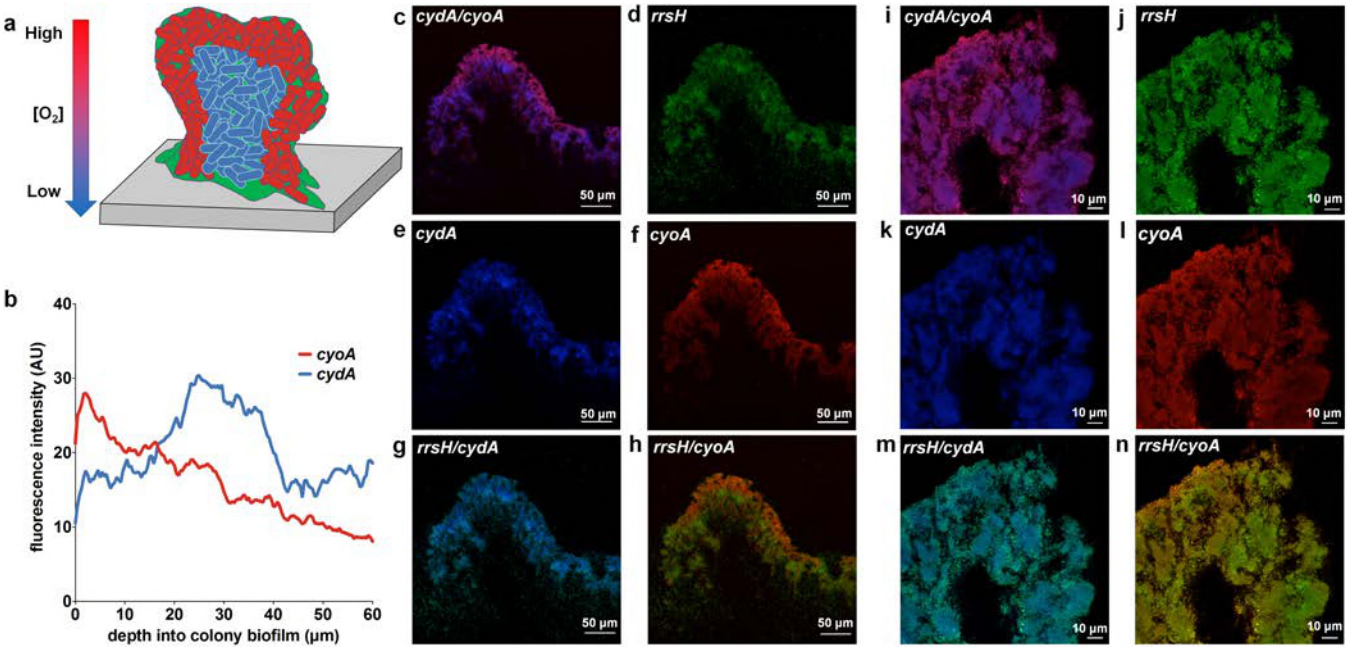

Figure 2: Expression of cytochrome oxidases as a function of the oxygen gradient. a, Cartoon depicting the detected localization of *cyoA* (red) and *cydA* (blue) transcripts in biofilm cryosections. **b,** Fluorescence intensity of *cyoA* and *cydA* PNA-FISH probes were quantified on ImageJ. Data are presented as the average fluorescence intensity as a function of depth obtained from four images, each with five measurements per image. **c – n,** Representative images of PNA-FISH stained biofilm cryosections at 20x magnification (**c – h**) and 63x magnification (**i – n**). Cryosections were stained with PNA-FISH probes targeting *cyoA* and *cydA* with *rrsH* (16S rRNA) as an endogenous control. Images are representative of three biological replicates.

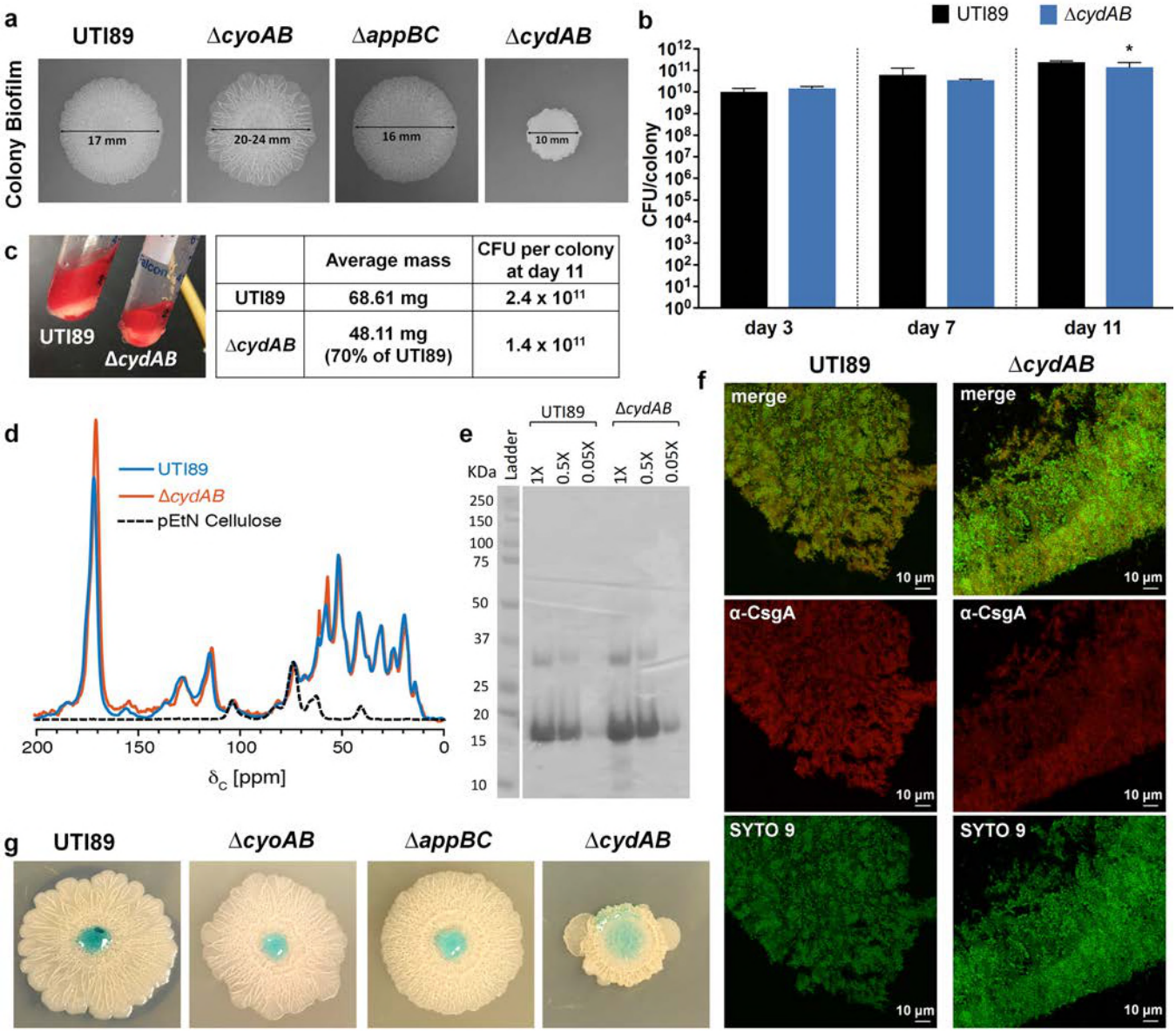

Figure 3. Cytochrome *bd* organizes biofilm architecture and ECM production. a, Colony biofilms of UTI89 and cytochrome oxidase mutants grown on YESCA agar for 11 days. Images are representative of at least 30 biological replicates. **b,** CFU per colony biofilm was measured at days 3, 7, and 11 of growth. Statistical analysis was performed in GraphPad Prism using a two-tailed unpaired t test. * = $p < 0.05$. Data are presented as mean ± SD. Data are representative of five biological replicates. **c, left,** Image depicting gross changes to extracellular matrix (ECM) abundance between UTI89 and Δ*cydAB* colony biofilms. ECM is stained red by the presence of Congo Red in the growth medium. **right**, Table lists average mass and CFU per colony biofilm after 11 days of growth. Average mass is from a pooled analysis of 186 individual colonies. CFU per colony is the average of five biological replicates. **d,** Solid-state NMR spectra of the ECM of UTI89 (blue), Δ*cydAB* (orange), and isolated pEtN cellulose (black). **e,** SDS-PAGE gel of UTI89 and Δ*cydAB* ECM. **f,** Immunofluorescence images of curli (α-CsgA, red) localization in UTI89 and Δ*cydAB* colony biofilm cryosections. **g,** Colored water droplets were added to the top of day 11 colony biofilms to probe biofilm barrier function.

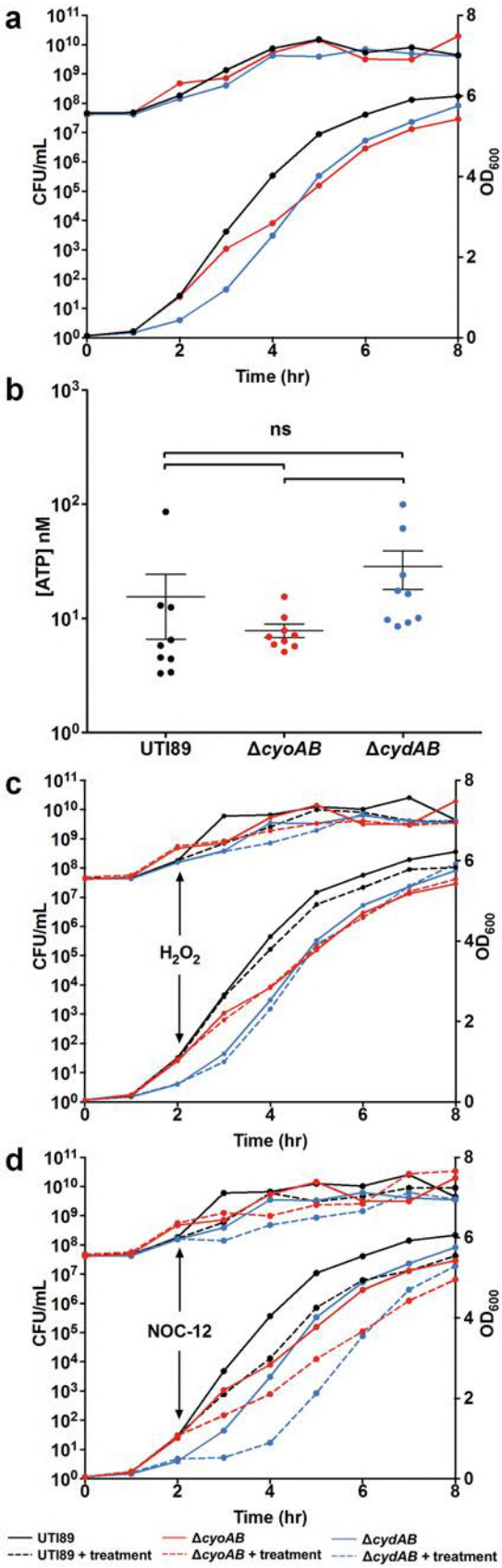

Figure 4: Cytochrome *bd* provides nitrosative stress resistance. a, Growth curves for UTI89, Δ*cyoAB*, and Δ*cydAB* as measured by CFU per mL (upper lines, left axis) and OD_{600} (lower lines, right axis). **b,** ATP levels measured from logarithmic cultures of UTI89, Δ*cyoAB*, and Δ*cydAB.* Statistical analysis was performed on GraphPad Prism using a two-tailed unpaired t test. Data are presented as mean ± SEM. **c – d,** Growth curves for UTI89, Δ*cyoAB*, and Δ*cydAB* as measured by CFU per mL (upper lines, left axis) and OD_{600} (lower lines, right axis). 0.5 mM of nitric oxide donor NOC-12 (**c**) or 1 mM hydrogen peroxide (**d**) was added at t = 2 hours. All data are representative of at least three biological replicates.

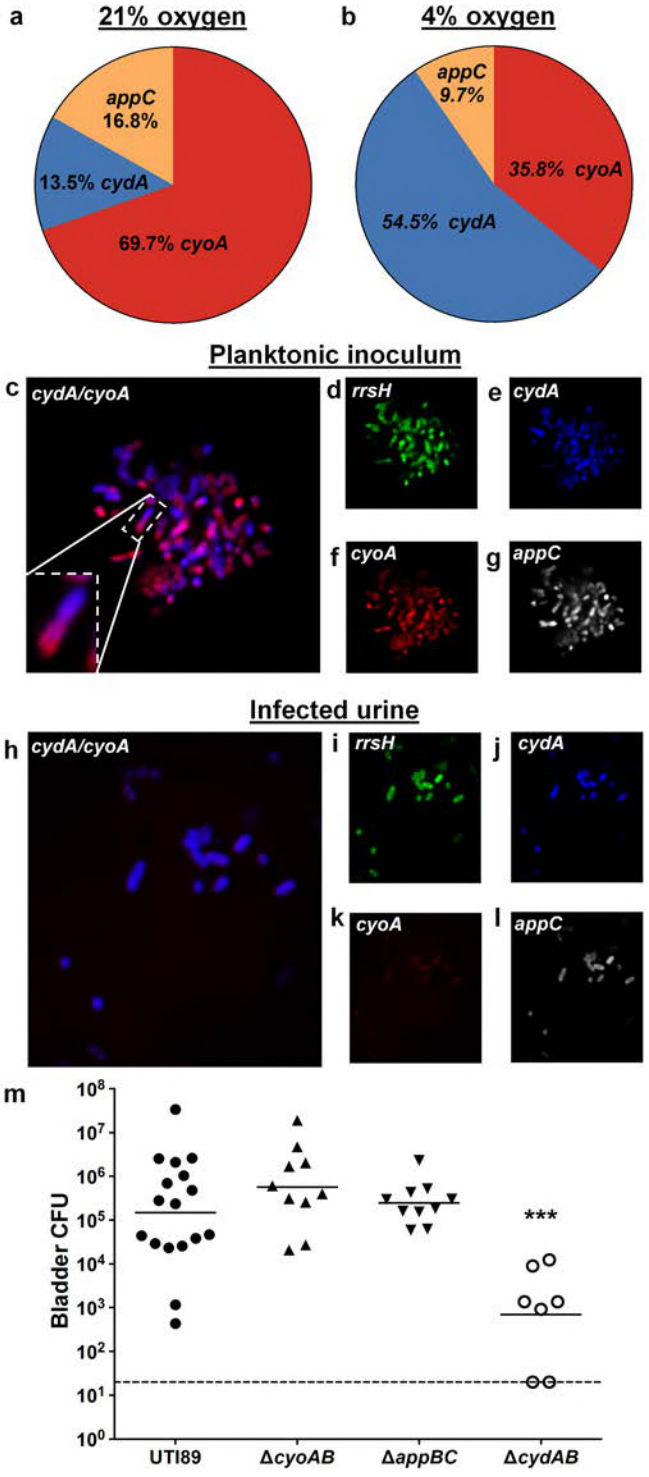

Figure 5: Respiratory heterogeneity provides a fitness advantage during urinary tract infection. a – b, Pie charts depicting relative abundance of *cydA*, *cyoA*, and *appC* transcripts detected using RT-qPCR in planktonic cultures grown at 21% oxygen in the manner used to prepare cultures to inoculate mice (**a**), as well as planktonic cultures grown at 4% oxygen (**b**)**.** Data is representative of three biological replicates. **c – g,** PNA-FISH was used to detect cytochrome oxidase transcripts from cultures used to inoculate mice. Data is representative of three biological replicates. **h – l,** PNA-FISH was used to detected cytochrome oxidase transcripts in the urine of mice infected with UTI89. Urine was pooled from 20 mice. **m,** Graph depicting bladder titers obtained from mice infected with UTI89 or cytochrome oxidase mutant strains at 24 hours post infection. Each point represents a mouse. UTI89 and Δ*cydAB* are representative of two independent experiments. Δ*cyoAB* and Δ*appBC* are representative of one experiment. Statistical analysis was performed in GraphPad Prism using a two-tailed Mann-Whitney test. Line represents geometric mean. *** = p< 0.001.

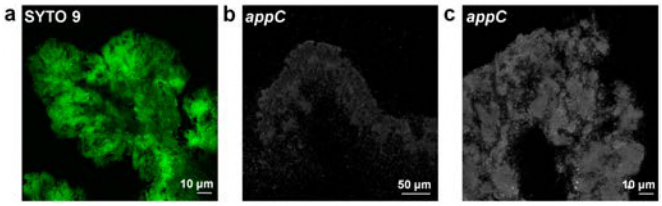

Figure S1: Localization of *appC* transcript in biofilm cryosections. a, Representative image of SYTO 9 stained biofilm cryosection at 20x magnification. **b – c,** Representative images of biofilm cryosections stained with an *appC* PNA-FISH probe at 20x (**b**) and 63x (**c**) magnification.

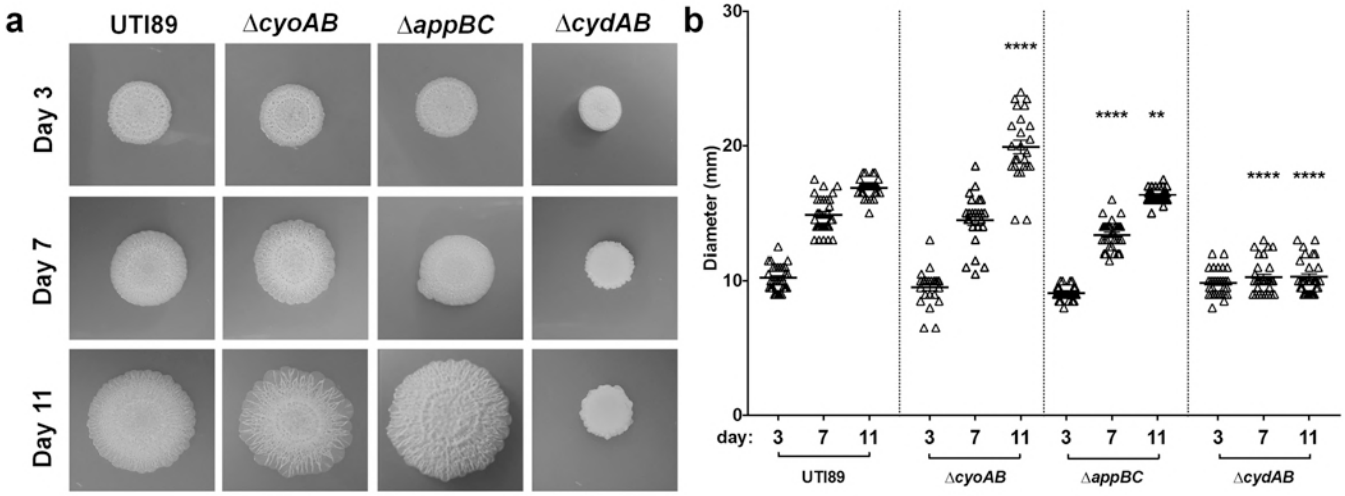

Figure S2: Temporal development of colony biofilms by UTI89 and isogenic cytochrome oxidase mutants. a, Representative images of UTI89 and cytochrome oxidase mutant colony biofilms grown on YESCA agar taken on day 3, 7, and 11 of growth. **b,** Graph depicting colony biofilm diameter at day 3, 7, and 11 of growth. Each triangle represents an individual colony biofilm. Data is representative of at least 30 biological replicates. Statistical analysis was performed in GraphPad Prism using Welch's t test. * = $p < 0.05$, ** = $p < 0.01$, *** = $p < 0.001$, **** = $p < 0.0001$.

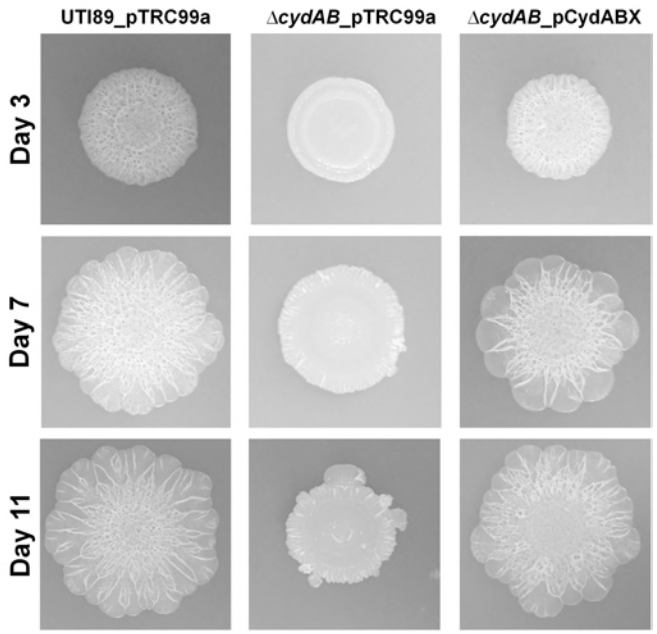

Figure S3: Extrachromosomal complementation of Δ*cydAB* rescues biofilm defects. Representative images on UTI89_pTRC99a, Δ*cydAB*_pTRC99a, and complemented Δ*cydAB*_pCydABX under the control of a native promoter. Images were taken of colony biofilms grown on YESCA agar at days 3, 7, and 11 of growth. Images are representative of at least 5 biological replicates.

Supplemental Movies S1-4: Cytochrome *bd* influences matrix hydrophobicity and resistance to penetration by aqueous solutions. Videos of colored water applied adjacent to a day 11 colony biofilm to assess the degree to which colony biofilms uptake aqueous solutions. **Movie S1,** UTI89; **Movie S2,** Δ*cyoAB*; **Movie S3,** Δ*appBC*; **Movie S4,** Δ*cydAB.* Videos are representative of at least 5 biological replicates.

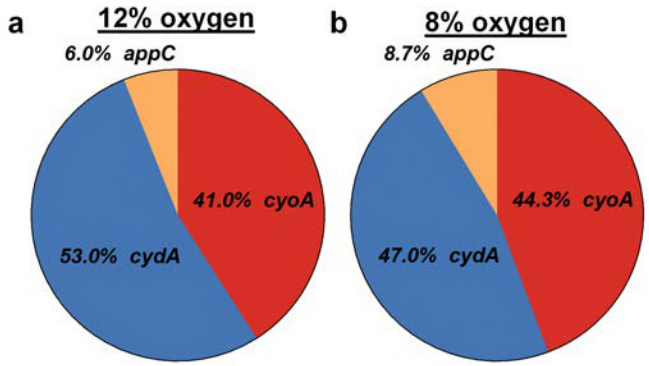

Figure S4: Ambient oxygen concentration influences cytochrome oxidase transcript abundance. Pie charts depicting relative abundance of *cydA*, *cyoA*, and *appC* transcripts detected using RT-qPCR in planktonic cultures grown at 12% (**a**) or 8% oxygen (**b**)**.** Data is representative of three biological replicates.

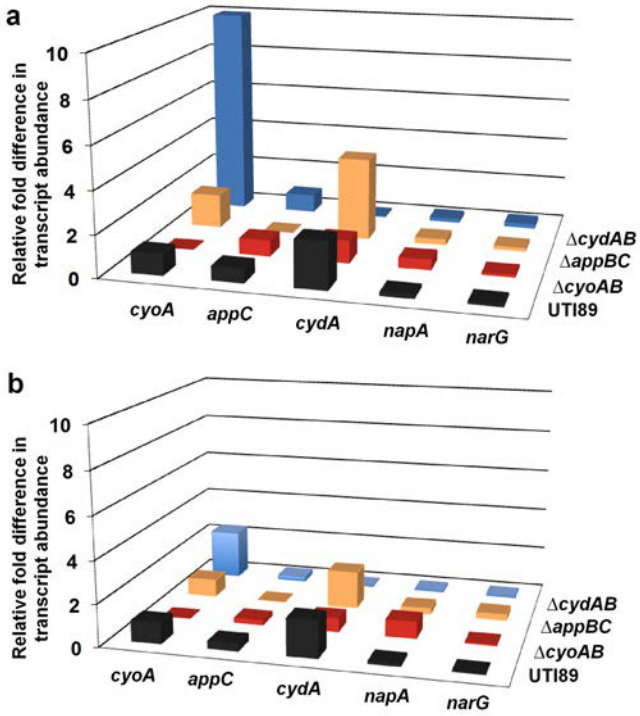

Figure S5: Expression of respiratory complexes in colony biofilms of cytochrome oxidase deletion mutants. RT-qPCR data depicting relative fold difference in respiratory transcript abundance in the center (**a**) and periphery (**b**) of day 11 colony biofilms across cytochrome oxidase mutant strains. In UTI89 (black), data is presented as relative fold difference in transcript abundance as compared to *cyoA* abundance. In each mutant strain, data is presented as relative fold difference in transcript abundance as compared to transcript abundance in UTI89.

Table S1: Primers and probes

Primer/Probe	Sequence (5' → 3')	Purpose
cydA_KO_Fwd	ATGATGTTAGATATAGTCGAACTGTCGCGCTTACAGTTT GCCTTGACCGCGATGTACGTGTAGGCTGGAGCTGCTTC	*cydAB* knockout
cydB_KO_Rev	GTTACGTTCAATATCTTCTTTGGTGATACGACCGAACATT TTCCAGTCATATGAATATCCTCCTTAG	*cydAB* knockout
cydA_KO_Test_Fwd	GATCAAATTGGTGAGATCGTGAC	*cydAB* knockout
cydB_KO_Test_Rev	CTAACAGAAGTGCCATCACG	*cydAB* knockout
cydA1_Fwd_XbaI	CTGCAGTCTAGACTGGTCAAGTTATCCATCATTCACT	*cydABX* complementation
cydX_Rev_SacI	CGTATTGAGCTC/TTGCGATAATCTTACTCATCAGATGTC	*cydABX* complementation
appC_KO_Fwd	ATGTGGGATGTCATTGATTTATCGCGCTGGCAGTTTGCT CTGACCGCGGTGTAGGCTGGAGCTGCTTC	*appBC* knockout
appB_KO_Rev	TTAGTACAGCTCGTTTTCGTTACGGCGGAGAGTTTCTGT CGTCATGCCATATGAATATCCTCCTTAG	*appBC* knockout
appC_KO_Test_Fwd	ACGCAGACGTCACGGCG	*appBC* knockout
appB_KO_Test_Rev	TGCACAGTCAGGTGCCAGC	*appBC* knockout
cyoB_KO_Fwd	TCAGTTGCCATTTTTCAGCCCTGCCTTAGTAATCTCATC GGTGTAGGCTGGAGCTGCTTC	*cyoAB* knockout
cyoA_KO_Rev	GTCATTATTTGCAGGCACTGTATTGCTCAGTGGCTGTAA TTCTGCGCTGCATATGAATATCCTCCTTAG	*cyoAB* knockout
cyoB_KO_Test_Fwd	CATCCAGATAAGACCGGAAGTG	*cyoAB* knockout
cyoA_KO_Test_Rev	GCAACATATGTGACCTGATAGC	*cyoAB* knockout
cyoA_Fwd	CAATGCCCTGTTCCGGGTAGATG	qPCR
cyoA_Rev	ACGGTACCTATCTTAATCATCATCTTCC	qPCR
cyoA probe	NED-TCGTCGTGTGCCAGCGGCTTG	qPCR
appC_Fwd	CGATGTCGCATTACGCTCG	qPCR
appC_Rev	GGTGCAGGTTCTGTTTGCCACT	qPCR
appC probe	NED-CTGCGTATGAAGTCGCGCAAG	qPCR
cydA_Fwd	GTGGCTACCGGTCTGACCATG	qPCR
cydA_Rev	CCAACCGAAGAAGAACAGACCTAC	qPCR
cydA probe	FAM-CGCTGGCAATCGAAGGTCTGATG	qPCR
narG_Fwd	TCTCGCTATACTGGACACCTGA	qPCR
narG_Rev	CCGTATAGTCCACCGGATTCAT	qPCR
narG probe	NED-TGCCGTCTGCGCCGCAGT	qPCR
napA_Fwd	CTTCCGCGTGTGGTACTGC	qPCR
napA_Rev	GTGCCGCTCGGGATATTCC	qPCR
napA probe	FAM-CGTCTGCCTGCGGACATGGTGGTGAC	qPCR
gyrB_Fwd	GATGCGCGTGAAGGCCTGATTG	qPCR
gyrB_Rev	CACGGGCACGGGCAGCATC	qPCR
gyrB probe	VIC-ACGAACTGCTGGCGGA	qPCR
cyoA PNA	CGTCGTGTGCCA – Lys (Atto425)	PNA-FISH
cydA PNA	CGATTGCCAGCG – Lys (Cy5)	PNA-FISH
appC PNA	TGCGCGACTTCATA – Lys (TexasRed)	PNA-FISH
rrsH PNA	AGTAATTCCGATTAACG – Lys (Atto532)	PNA-FISH